Progressive mural cell deficiencies across the lifespan in a *foxf2* model of Cerebral Small Vessel Disease

Merry Faye E. Graff, Emma E.M. Heeg and Sarah J. Childs*

[1] Alberta Children's Hospital Research Institute, University of Calgary, T2N 4N1, Canada.
[2] Department of Biochemistry and Molecular Biology, University of Calgary, T2N 4N1, Canada.

*Corresponding author email: schilds@ucalgary.ca.

Sarah Childs ORCID iD: https://orcid.org/0000-0003-2261-580X.
Merry Faye Graff ORCID iD: https://orcid.org/0009-0006-6861-5759
Emma Heeg ORCID iD: https://orcid.org/0009-0002-0879-133X

Keywords: Foxf2, Pericytes, Mural Cells, Zebrafish, Vascular Stability, Small Vessel Disease

Abstract (250 words)

While developmental origins are suspected for many adult diseases, the lifespan effects of developmental perturbations have not been well studied. Cerebral Small Vessel Disease (SVD) is a leading cause of stroke and dementia and yet is often an incidental finding in aged patients due to the inaccessibility of brain vasculature to imaging of small vessels. In humans, reduced *FOXF2* is associated with an increased stroke risk and SVD. We use a zebrafish partial *foxf2* loss of function to model its effect on small vessel biology through development and aging. In the zebrafish, *foxf2* is expressed in brain vascular pericytes and promotes vascular stability. We find that the initial pool of pericytes in developing *foxf2a* mutants is strongly reduced without affecting the endothelial network. The few brain pericytes present in mutants have strikingly longer processes and enlarged soma. *foxf2a* mutant pericytes can partially repopulate the brain after genetic ablation suggesting some recovery is possible. Nonetheless, adult *foxf2a* mutant brains show regional heterogeneity, with areas of normal pericyte coverage of vessels, but others with severe pericyte depletion. Both pericyte and endothelial morphology is strongly affected in adults. Taken together, *foxf2a* mutants fail to generate a sufficient initial population of pericytes and the few pericytes remaining have abnormal cell morphology. Over the lifespan *foxf2*a loss leads to severely abnormal cerebrovasculature. Our work opens new understanding of the progression of genetic forms of human Cerebral Small Vessel Disease.

Introduction

Brain microvessels supply billions of neurons and brain cells with required oxygen and nutrients. Pathologies affecting brain microvasculature progress slowly and silently over a lifetime but have devastating consequences from decreased perfusion and vascular destabilization. Cerebral small vessel disease (CSVD) encompasses progressive heterogeneous changes in brain microvessels; it is the most common cause of vascular dementia and a significant contributor to stroke and cognitive decline (Østergaard et al., 2016). 25% of all strokes are the result of CSVD, yet effective targeted treatments remain elusive (Østergaard et al., 2016). This is in part due to the inability to both detect and assess progressive damage in the brain.

While there are several genes implicated in familial CSVD (i.e., *NOTCH3*, *HTRA1*, *FOXC1*, *COL4A1* and *COL4A2*), there is a lack of suitable *in vivo* models for studying disease development and progression. Research has predominantly focused on *NOTCH3*, but within the last decade, *FOXF2* has emerged as a risk locus involved in CSVD (Chauhan et al., 2016; Duperron et al., 2023). SNPs in the intergenic region between *FOXF2* and *FOXQ1* decrease *FOXF2* expression and significantly increase stroke risk due to the variant decreasing efficiency of *ETS1* binding to a novel *FOXF2* enhancer (Ryu et al., 2022).

Foxf2 promotes mural cell differentiation and vascular stability in the zebrafish brain and is expressed highly in brain pericytes, (Ahuja et al., 2024; Chauhan et al., 2016; Reyahi et al., 2015; Ryu et al., 2022). Brain pericytes interact closely with endothelial cells, contributing to extracellular matrix (ECM) deposition and blood-brain barrier (BBB) formation, in addition to providing vasoactivity and stability (Bahrami and Childs, 2020; Daneman et al., 2010; Dave et al., 2018; Stratman et al., 2009). In animal models, an absence of brain pericytes results in hemorrhages and accelerates vascular-mediated neurodegeneration (Bell et al., 2010; Wang et al., 2014). Foxf2 is clearly important for vascular stability across species, as loss of Foxf2 in mice and zebrafish leads to increased brain hemorrhage and alterations in brain pericyte numbers and differentiation (Chauhan et al., 2016; Reyahi et al., 2015; Ryu et al., 2022). Brain tissue from patients with aging-related dementias (i.e. post-stroke dementia, vascular dementia, Alzheimer's disease) has reduced deep white matter pericytes and associated BBB disruption (Ding et al., 2020) suggesting that pericytes should be examined as mediators of CSVD progression in patients with FOXF2 deficiency.

Genome-wide association (GWA) indicates that carrying a minor allele of an SNP in a *FOXF2* enhancer leads to reduced, but not absent, FOXF2 and is associated with stroke (Ryu et al., 2022). For this reason, we model CSVD using a zebrafish with reduced Foxf2 dosage.

Strikingly, while pericytes in embryonic *foxf2* mutants are clearly affected, *foxf2* mutants can survive until adulthood, albeit with a reduced lifespan. How pericytes change across the lifespan while CSVD progresses is unknown.

Here we find that *foxf2a* mutants have significantly reduced brain pericyte numbers as embryos that do not recover over time. Pericytes in mutant embryos and larvae exhibit morphological abnormalities such as increased soma size, process length and degeneration. We show that processes and soma in the adults are also abnormal, though their morphology differs over the lifespan. Although the initial pool of pericytes is smaller, mutants can regenerate pericytes after ablation. Our analysis suggests that *foxf2* is required within pericytes to modulate numbers but also has a strong effect on morphology. We show that brain pericytes may contribute to the pathological progression of genetic CSVD, starting in embryonic development and continuing across the lifespan. Understanding the early developmental aspects of late-onset vascular conditions like CSVD will aid in the development of effective therapeutic strategies.

Results

Pericyte number is consistently lower in foxf2 mutant embryos and larvae

We have previously described reduced pericyte numbers in *foxf2a*^{ca71}; *foxf2b*^{ca21} double homozygous mutants in late embryogenesis at 3 days post fertilization (dpf) (Ryu et al., 2022). Stroke susceptibility in humans is associated with reduced, but not absent, FOXF2 expression. Therefore, to better model progressive cerebrovascular defects that might occur with human FOXF2 deficiency, we developed single homozygous *foxf2a* mutants as a model of reduced dosage. Zebrafish *foxf2a* and *foxf2b* genes are the result of genome duplication in zebrafish ~430 million years ago, and have similar gene expression (Arnold et al., 2015; Chauhan et al., 2016). We have detected no difference in function between the two genes, and therefore for this study, we consider *foxf2a* loss of function to be similar to human heterozygous loss of FOXF2 function, a state that is observed in the population in GnomAD (Chen et al., 2024).

To understand phenotypic evolution, serial imaging of individual brains of *foxf2a* mutants at embryonic stages (3 and 5 dpf), and at larval stages (7 and 10 dpf) was undertaken. Mutants were live-imaged using endothelial *(kdrl:mCherry)* and pericyte *(pdgfrβ:Gal4, UAS:GFP)* transgenic lines. Brain pericytes are closely associated with and extend processes over the endothelium in the midbrain and hindbrain of zebrafish (Fig. 1A-A''). In wildtype embryos, the number of pericytes increases progressively from 3 through 10 dpf (Fig. 1B). *foxf2a* mutants show significantly fewer pericytes on brain vessels at 3 dpf (Fig. 1C; mean 21 in wildtype and 10

in mutants). The pericyte deficiency continues through 5, 7, and 10 dpf (Fig. 1C-D), and although it has variable penetrance, mutant brains with the most pericytes are at best similar to wildtype brains with the fewest pericyte numbers. The same pattern of pericyte reduction is seen *foxf2a* mutants from a heterozygous incross suggesting there is no maternal effect (Fig. 1E-F). Abnormal coverage varies among mutant larvae. However, mutants with regional absence in earlier stages, have coverage defects that persist into later stages, suggesting the initial population of pericytes is a key player in extended coverage (Fig. S1).

Double *foxf2a;foxf2b* mutants also have significantly fewer brain pericytes in mutants than wildtype at every stage (Fig. S2A-B; mean 19 in the wildtype and 9 in mutants at 3 dpf) and have a fully penetrant phenotype (Fig. S2C). Incomplete penetrance in *foxf2a* single mutants is likely due to variations in *foxf2b* expression among different embryos, as loss of both genes is fully penetrant.

Although we focus on mural cells, Foxf2 is expressed in adult mouse brain endothelium (Vanlandewijck et al., 2018). We assessed *foxf2a* and *foxf2b* mRNA expression patterns using HCR *in situ* hybridization. At 3 dpf, *foxf2a* is co-localized with the pericyte marker *ndufa4l2a* in the brain (Fig. 2A). *foxf2a* also shows low expression in brain endothelium, co-localizing with the blood vessel marker *kdrl* (Fig. 2A). The expression pattern of *foxf2b* was comparable, with localization observed in pericytes (indicated by *pdgfrβ*) and only weakly in ECs (indicated by *kdrl*) (Fig 2B). This is supported by the DanioCell atlas of single-cell sequencing of multiple embryonic stages that shows expression is strongest in mural cells, pericytes and vascular smooth muscle cells and low in endothelial cells (Sur et al., 2023) (Fig. S3). Thus, while *foxf2a* and *foxf2b* are principally expressed in pericytes they have some expression in endothelium during brain development. Pericyte loss or impairment leads to alterations in vascular patterning in the mouse retina (Eilken et al., 2017). To assess if the endothelial network is affected in *foxf2a* mutants, we employed a Python workflow using Vessel Metrics (McGarry et al., 2024) (Fig. 2C). We found no statistical difference in total network length between wildtype and mutants at 3 dpf (Fig. 2D) or hindbrain CtA diameter (Fig. 2E). However, pericyte density (number of pericytes divided by the total network length) is reduced by 40% in *foxf2a* mutants (Fig. 2F), reflecting the loss of pericytes with no change in vessel network length. Similarly, the coverage of pericytes on vessels (total process coverage from brain pericytes divided by the total network length) is reduced by 39% in mutants (Fig. 2G). Our data suggests that *foxf2a* depletion predominantly affects embryonic pericytes and not endothelial patterning in developing zebrafish.

Early defects in brain vasculature have lifelong consequences.

foxf2 mutant animals can survive to adulthood, albeit with a reduced lifespan (~1 year instead of >2 years). Are early pericyte deficiencies repaired, or is loss of pericytes unimportant to survival and reproduction, at least to middle-aged adulthood? To understand how early defects in brain pericyte numbers evolve over the lifespan, we dissected adult wildtype and *foxf2a* mutant brains (Fig. S4A). Gross measurements of standard length (snout to tail) show no significant differences between wildtype and mutants (Fig. S4B) except for female mutant brain length and width is significantly smaller at 11 months post fertilization (mpf) (Fig. S4C-D). However, there is no significant difference in the proportional brain: standard length ratio in *foxf2a* mutants vs. wildtype (Fig. S4E).

To visualize brain pericytes and endothelium in their 3D environment, the dissected brains on pericyte and endothelial double transgenic backgrounds at 3 months post fertilization (mpf), were cleared, stained for GFP and mCherry and imaged using light sheet microscopy. A projected 3D view of the whole brain shows striking defects in pericyte density and coverage (Movie 1-2; Fig. 3A-B). Pericyte morphology is altered, and blood vessel density is visibly reduced in mutant brains (Fig. 3C-D).

We imaged cleared dissected brains at 11 mpf and find similarly striking defects using 3D whole-brain projections (Fig. 3E). At the cellular level, pericyte coverage and morphology is altered (Fig. 3F). In the wildtype brain, adult pericytes have a clear oblong cell body with long, slender primary processes that extend from the cytoplasm with secondary processes that wrap around the circumference of the blood vessel. These pericytes form a continuous network of processes to cover the blood vessels in the brain. In *foxf2a* mutant adult brains, pericyte soma lose their oblong shape and cell bodies cannot easily be differentiated from processes. Mutant cells also extend thickened linear processes, with no secondary processes encircling the vessels. Mutant pericytes do not form an extensive network with other neighbouring pericytes. We note that there is variable phenotypic penetrance in *foxf2a* adults that is reflective of the incomplete penetrance in *foxf2a* embryos (Fig. S5).

To view cellular morphology, we sectioned adult brains and immunolabeled pericytes and endothelium. In wildtype adult brains, we identified three subtypes of pericytes, ensheathing, mesh and thin-strand, previously characterized in murine models (Berthiaume et al., 2018a) (Fig. S6). In comparing brain sections from both wildtype and *foxf2a* mutants, we observe a reduction in brain pericytes and these pericytes have an unusual morphology. On smaller vessels, mutant pericytes exhibit more linear processes with barely distinguishable soma, markedly differing from the characteristic appearance of wildtype adult pericytes (Fig.

4A). Similarly, *pdgfrβ*-expressing cells on large calibre vessels (mural cells, likely vSMCs) show a drastic alteration in morphology and coverage (Fig. 4B). Though mutant embryos do not have evident abnormalities in their endothelium, large, aneurysm-like structures are evident in the adult brain (Fig. S7). These structures also appear to have decreased *kdrl* expression. Thus, both wholemount and sectioned tissue show that brain vascular mural cell number and morphology is drastically impacted in adult *foxf2a*$^{-/-}$ mutant brains, with increasing involvement of the endothelium, suggesting a worsening phenotype throughout life.

Morphological abnormalities emerge in the larval brain of mutants.

Considering the altered pericyte morphology of adult mutants, we revisited developmental stages to identify when these abnormalities first arise. We analyzed morphology at 3 and 10 dpf using in vivo confocal imaging to understand defects in the cell body (soma) and processes (Fig. 5A). We find no significant difference in the soma area at 3 dpf, but at 10 dpf, there is a significant increase in mutant pericyte soma area compared to wildtype (Fig. 5B). In parallel, wildtype pericytes undergo a slight reduction in soma size from 3 to 10 dpf.

The low number of brain pericytes in *foxf2a* mutants means that distinct pericyte processes can be distinguished and measured. However, in wildtypes, pericyte processes are not easily distinguished. For accurate process length measurements in wildtype we used multispectral labelling with a pericyte-specific Zebrabow transgenic line *(pdgfrβ:Gal4, UAS:Zebrabow)* (Pan et al., 2013; Whitesell et al., 2019). Cre mRNA was injected at the one-cell stage to activate random recombination, allowing us to visualize individual neighbouring pericytes (Fig. 5C). Wildtype processes have a mean length of 81.3 µm vs 102.9 in the mutant at 3 dpf and 96.3 µm vs 147.6 in the mutant at 10 dpf (Fig. 5D). Thus, the pericyte process lengths of *foxf2a* mutants are significantly increased at 3 and 10 dpf (Fig. 5D).

We observed some differences from published analysis of the behaviour of adjacent pericyte processes. In zebrafish development, interactions between adjacent pericytes varied from no contact to slight overlap (Fig. 5E). While direct contact with no overlap is the most common interaction (similar to mouse adult brain pericytes (Berthiaume et al., 2018b)) (Fig. 5F), there are examples of overlap. The average overlap between wildtype pericyte processes at 10 dpf was 5.9 µm (Fig. 5G). Together, these observations revealed previously unseen pericyte process behaviours in wildtype animals.

To further explore mutant pericyte behaviour, we conducted serial imaging during larval development. Over time, some mutant pericyte processes form disconnected bead-like blebs with cell bodies that disappear over time (Fig. 6A). This pericyte phenotype can occur on

vessels with full patency and is not associated with endothelial regression. The bead-like remnants are highly prevalent during larval development in *foxf2a*$^{-/-}$ mutants but not present in wildtype (Fig. 6B). To visualize process degeneration in real-time, we time-lapse imaged from 4-5 dpf (Fig. 6C). The pericyte can undergo a process reminiscent of cell death with soma blebbing and process degeneration phenotypically resembling neural dendrite degeneration or pruning (Fig. 6D).

In summary, *foxf2a* mutant pericytes show reduced numbers, increased soma size, and elongated processes with evidence of abnormal process degeneration during larval development. In addition, we make the novel observation of overlapping pericyte processes during zebrafish development.

Foxf2a mutants do not have an impaired capacity to repopulate brain pericytes.

Zebrafish are known to have regenerative capacity in various tissues (Becker et al., 1997; Lepilina et al., 2006; Otteson and Hitchcock, 2003), yet *foxf2a* mutant embryos that are pericyte-deficient maintain strong brain pericyte defects through aging. We next tested whether *foxf2a* mutants lack the capacity to regenerate pericytes. We reduced pericyte numbers in a *foxf2a* heterozygous incross using a cell ablation strategy. Zebrafish expressing *pdgfrβ:Gal4, UAS:NTR-mCherry* and *flk:GFP* transgenes were treated with 5 mM metronidazole (MTZ) at 50 hpf for 1 hour which ablates most pericytes. MTZ is a prodrug substrate that elicits cell death in nitroreductase (NTR)-expressing cells due to its cytotoxic derivatives. We then imaged and counted brain pericytes at 3 dpf (a day after treatment) and 10 dpf (recovery).

At 3 dpf, in the vehicle (DMSO) control group there is the expected significant difference between wildtype and mutant pericyte numbers (Fig. 7A-B). Both mutants and wildtypes have a severe reduction in pericytes at 3 dpf post-ablation, and are not significantly different from each other (Fig. 7B). By 10 dpf, pericytes are partially repopulated in both wildtype and mutant ablated groups (Fig. 7C). Surprisingly, given the initial pericyte number defects in *foxf2a* mutant embryos, we find no significant difference between any groups (Fig. 7D; mean 70 in wildtype DMSO treated, 53 in mutant DMSO treated, 43 in wildtype MTZ treated, 33 in mutant MTZ treated). This shows that *foxf2a* mutants retain their ability to repopulate pericytes following ablation. Thus, while *foxf2a* mutant pericytes are able to regenerate following induced catastrophic loss, in uninjured animals, the recovery process cannot fully compensate for the depleted pericyte pool in early development.

Discussion

Our reduced dosage model of Foxf2 demonstrates disease processes at cellular and molecular levels in intact animals, giving insight into pathological changes that occur during CSVD that have not been observed in other models or humans. Our data supports a developmental origin in this model of CSVD that progresses and evolves across the lifespan (Fig. 8).

Dosage sensitivity of Foxf2

The logic for using a reduced dosage of Foxf2 in our studies is to better match the effect of common population variants leading to CSVD. We previously modelled the effect of a high-risk CSVD and stroke-associated SNV on the expression of FOXF2 in human cells, showing that it can reduce expression by ~50% (Ryu et al., 2022). Because there are two *FOXF2* orthologs in zebrafish (*foxf2a* and *foxf2b*), *foxf2a* homozygotes have equivalent FOXF2 dosage as human heterozygotes. Foxf2 is highly dosage sensitive, zebrafish *foxf2a* hets show a significant reduction in brain pericytes, demonstrating a phenotype with a loss of only 25% gene expression. For the phenotypes we examine, *foxf2a* can be incompletely penetrant, while *foxf2a;foxf2b* double mutants are fully penetrant suggesting that variations in *foxf2b* compensate and lead to differences in penetrance. Genetic compensation is common with gene duplication (Kok et al., 2015; Rouf et al., 2023) and would explain variability in disease phenotypes in different individuals with the same mutation.

Impaired embryonic pericyte coverage in Foxf2 deficiency

We show that numbers of brain pericytes are reduced at all stages, embryonic to adult, in *foxf2a*$^{-/-}$ mutants. We cannot differentiate whether deficient numbers are due to changes in the pericyte precursor population (i.e. *nkx3.1* positive cells (Ahuja et al., 2024)) upstream of pericyte differentiation, or whether *foxf2a* deficient cells are unable to differentiate into *pdgfrβ* positive pericytes. The deficiency is significant at every stage, including 3 dpf, the earliest time point that pericytes are robustly observed in development. The pericyte deficiency is a primary phenotype, we do not find a significant difference in total vessel network length or hindbrain CtA diameter at 3 dpf in *foxf2a* heterozygotes or mutants. Pericytes provide contractility that maintains basal tone in the embryo from 4 dpf onwards (Bahrami and Childs, 2020). The result of having deficient pericyte numbers on a normal-sized endothelial network length is that pericyte density and coverage of vessels are significantly decreased. It is intriguing that pericyte process length is increased at both 3 and 10 dpf, and we hypothesize this might be an adaptation to low pericyte number.

A second morphological abnormality of *foxf2a* deficient pericytes is that their soma size is increased at 10 dpf. Pathological changes in soma size have not been observed in brain pericytes and the mechanisms behind hypertrophy remain unclear. Increased neuronal soma size is observed in Amyotrophic Lateral Sclerosis or Lhermitte-Duclos disease (Dukkipati et al., 2018; Kwon et al., 2001) and is linked to mTor signaling (Kwon et al., 2003). In neuronal populations, moderate soma swelling can be an adaptation for survival, while rapid, drastic swelling indicates imminent death (Rousseau et al., 1999). However, it is unclear whether this occurs in pericyte phenotypes.

Contributing to the reduction in pericyte numbers, we observe degeneration of pre-existing pericytes in *foxf2a* mutant but not wildtype animals. This degeneration phenotypically resembles neuronal dendrite remodelling and pruning during development (Fukui et al., 2012; Greenwood et al., 2007). Yet it remains unclear if these two distinct populations share similar degeneration mechanisms in response to stress or cellular damage.

Insights on fundamental pericyte process properties

The reasons behind the hypergrowth of pericyte processes in *foxf2a*$^{-/-}$ mutant brains is unclear. Berthiaume et al (2018a) propose that repulsive interactions among pericytes in the adult brain establish boundaries between adjacent pericytes, preventing their processes from overlapping. In this case, one might hypothesize that *foxf2a* mutant pericytes would lack the inhibitory signals normally provided by neighbouring pericytes during essential stages of development, leading to uncontrolled growth.

In mice, adult brain pericytes form a non-overlapping network along capillaries, although their processes occasionally approach each other without overlapping (Berthiaume et al., 2018b; Hill et al., 2015). Pericyte processes have not been studied in zebrafish or the developing brain. Strikingly, using multispectral (Zebrabow) labelling, we find that there is process overlap in the developing zebrafish brain. Overlaps occur on capillary segments and at branch points. Previous studies in mice were in the adult mouse brain, and it is possible that overlapping processes in the developing brain could be transient, zebrafish-specific, or they could have been overlooked in the mouse experiments. Testing how pericyte process interactions change during the lifespan would provide insights into the differences observed between these studies.

We have also observed forked extensions at the tips of some pericyte projections at 10 dpf in wildtype embryos, where pericytes are not in contact. Whether these unique structures are involved in attractive/repulsive signals between pericytes or help determine the direction and extent of process growth is unclear, but understanding the fundamental mechanisms governing pericyte-pericyte process interactions would yield valuable insights into development and disease.

Changes in foxf2a mutants across the lifespan

In adult brains, hypertrophic pericyte soma are no longer present; rather, soma take on very unusual, 'stiff' shapes and become almost indistinguishable from processes. The adult processes are more linear and shorter than embryonic processes. This may indicate that hypertrophic pericytes do not survive to adulthood or that they change their morphology over time. Given the limited knowledge in this area, the underlying factors driving this shift in pericyte morphology are unclear. Actin is present near the plasma membrane of cells, where it provides structural and mechanical support to allow for motility and determine structure. Given the abnormal shapes of adult pericytes, alterations in actin may contribute to their irregular morphology.

In the adult brain, abnormal *pdgfrβ*-expressing cells are observed on large-calibre vessels and likely represent vSMCs. These cells are also found in regions with aneurysm-like vessels, suggesting that vSMCs may lose functionality over time, leading to increased vulnerability of underlying vessels to dilation and weakening. Loss of *acta2* and, subsequently, vSMCs, has been associated with conditions such as thoracic aortic aneurysms and dissections (Guo et al., 2009). This suggests that loss of *foxf2* in small vessels potentially leads to compensatory mechanisms affecting vSMC structure and function as the organism matures.

In embryonic *foxf2* mutants, brain vessel diameter and network length are not significantly altered. However, abnormalities in vessel organization and *kdrl* expression are evident by adulthood. Our data suggests that *foxf2* deficiency contributes to cumulative vascular defects, further emphasizing the importance of this gene in maintaining proper brain vessel function and organization.

Initial pericyte pool and lifelong vascular health

We genetically ablated pericytes to test the ability for pericyte recovery. Surprisingly, there is no significant difference in pericyte numbers between ablated and non-ablated groups, nor between wild-type and mutant fish, and cells do not appear to be morphologically different, even with severe ablation. Thus, when placed under stress, *foxf2a* mutants can regenerate a portion of their pericytes; yet, under baseline conditions, they remain deficient. Our lab recently demonstrated that pericyte precursors are labeled by *foxf2a* before the establishment of well-known markers such as *pdgfrβ* (Ahuja et al., 2024). This raises the question of whether the original pericyte precursor pool has intrinsic defects due to the absence of *foxf2a* that is essential in the normal development of these cells. Determining whether there is a critical period for pericyte development—and whether early interventions could mitigate these deficits—will be key to understanding cerebrovascular resilience and potential therapeutic strategies. Our findings indicate that reduced *foxf2a* dosage leads to long-term cerebrovascular defects that arise early in development and persist throughout the lifespan, with early and late phenotypes with different morphologies. Further research into pericyte development, signaling pathways, and the impact of early vascular defects on disease progression will be crucial for developing strategies to prevent or treat cerebrovascular conditions.

Materials and Methods

Zebrafish Husbandry and Strains

All procedures were conducted in compliance with the Canadian Council on Animal Care, and ethics approval was granted by the University of Calgary Animal Care Committee (AC21-0169). Embryos were maintained in E3 medium (5mM NaCl, 0.17mM KCl, 0.33mM CaCl2, 0.33mM MgSO4, pH = 7.2) (Westerfield, 2007) at 28°C. Larvae up to 10 dpf were maintained in an incubator with a light cycle (14 hours light, 10 hours darkness), with daily water changes and feeding. All experiments included wildtype as a comparison group, and developmental stages, n's, and genotypes are noted for each experiment (Appendix A). All mutant and transgenic lines are listed in the Key resources table. For adult studies, equal numbers of males and female fish were analyzed.

Genotyping

Adult fish were anesthetized in 4% Tricaine (Sigma) and placed on a cutting surface. A small portion of the tip of the fin was clipped using a razor blade, and the fish were returned to the system to recover. For developmental DNA isolation, whole embryos, or larvae (up to 10 dpf) were anesthetized in 4% Tricaine.

Genomic DNA (gDNA) was extracted using the HotSHOT DNA isolation protocol, adapted from Kosuta et al., 2018. To isolate gDNA, tissue or embryo was placed in 50 µL of Base Solution and incubated at 95°C for 30 minutes. 5 µL of Neutralization Solution was added to neutralize the reaction. Samples were spun down in a mini centrifuge, and DNA was sampled from the top portion of the solution to avoid undigested samples.

Zebrafish were genotyped for target genes or the presence of transgenes (Table 2) using the KAPA2G Fast HotStart Genotyping Mix (Roche, KK5621), as per the manufacturer's instructions. *foxf2* mutants were genotyped using *foxf2a* primers (Fwd: ATG CAC TCG GCT CTC CAA AA; Rev: GAT CGC CAT GAC TAT CGG GG). A custom TaqMan probe for *foxf2b*^{ca22} (ANAACEC) was obtained from Applied Biosystems. Samples were genotyped using the QuantStudio 6 Flex Real-Time PCR System (Applied Biosystems) with the wildtype allele reported in FAM and the mutant allele reported in VIC.

Brain Dissection

Zebrafish were first euthanized in Tricaine and mounted on a Sylgard gel plate with dissection pins to stabilize them. Scissors were used to sever the brain stem completely at the base of the head posterior to the hindbrain. The eyes were removed with forceps/micro-scissors, and the optic stalks were cut. An incision was then made at the posterior portion of the skull plate anteriorly. Forceps were used to pull back the skull plate and orbital bones. Any nerve connections were severed, and the brains were removed and immediately fixed in ice-cold 4% PFA overnight at 4°C.

Brain Tissue Clearing

Whole zebrafish brains were cleared by either CUBIC (SusakWe et al., 2015), or iDISCO+ protocols. For CUBIC, samples were incubated in 1:1 ratio of Reagent 1 (25% Quadrol (Sigma, 122262), 25% Urea, and 15% TritonX-100):H2O overnight at 37°C. Next, brains were incubated in 100% Reagent 1 at 37°C until the tissue was transparent. Finally, brains were rinsed in PBS, mounted in 2% low melting point agarose and re-placed in 100% Reagent 1 at 37°C until the tissue was transparent.

For iDISCO, the samples were first dehydrated in methanol:H_2O dilution series for 30 minutes each, then chilled at 4°C. Next, samples were incubated overnight in a 1:3 ratio of dichloromethane (DCM; Sigma, 270997):methanol at room temperature. The following day, samples were washed in methanol and then chilled at 4°C before bleaching in fresh 5% H_2O_2 in methanol overnight at 4°C. Then, samples were rehydrated in methanol:H2O dilution series for 30 minutes each, then washed in PTx.2 (0.2% TritonX-100 in PBS) twice over two hours at room temperature. Next, samples were incubated in permeabilization solution (0.3 M glycine, 20% DMSO in 400 mL PTx.2) at 37°C for up to two days, after which the samples were rinsed in PBS twice over one hour. Samples were then washed three times over two hours in 0.5 mM SDS/PBS at 37°C for three days before being incubated in primary antibody (Table 2) in 0.5 mM SDS/PBS at 37°C for two more days. The primary antibodies were refreshed in PTx.2 and left for another 4 days before overnight washing in PTwH (10 µg/ml heparin and 0.2% Tween-20 in PBS) at 37°C. Samples were left in secondary antibodies (Table 2) in PTwH/3% NSS at 37°C for 3 days, refreshed and left for another 3 days before washing overnight in PTwH. After immunolabeling, brains were mounted in 2% LMA and dehydrated in methanol:H_2O dilution series for 30 minutes each and left overnight at room temperature. Next, brains were incubated in a 1:3 ratio of DCM: methanol at room temperature for three hours before washing in 100%

DCM for 15 minutes twice. Finally, brains were incubated in Ethyl cinnamate (Sigma, NSC6773) for two hours before replacing the solution and incubating overnight at room temperature.

Tissue Sectioning

For vibratome sections, brains were fixed in 4% PFA, washed and mounted in 4% Low Melt Agarose (Invitrogen, 16520-050) before sectioning with a vibratome (Leica, VT1000S) to obtain a series of transverse sections at 50 µm.

Immunofluorescence

Sections for immunofluorescence were briefly washed in PBS, followed by 2% TritonX-100 in PBS for permeabilization. Sections were moved from the permeabilization solution into blocking buffer (5% Goat serum, 3% BSA, 0.2% TritonX-100 in PBS) for 1 hour before incubation in primary antibody (Table 2). Sections were then washed and left in secondary antibodies (Table 2) for 3 hours at room temperature. After incubation, sections were washed, mounted and cover slipped with Fluoromount-G™ Mounting Medium, with DAPI (Invitrogen, E141201) or without counterstain (ThermoFisher, 00-4958-02). Antibodies are listed in the Key Resources Table.

Drug Treatments

Embryos were dechorionated prior to treatment, and all drug treatments had DMSO added to an equivalent concentration as the drug solution as a control (Sigma, D8418-100ML) and were performed in a 24-well plate with approximately 15 embryos per well. For pericyte ablation experiments 5 mM Metronidazole (MTZ; Sigma, M3761) was applied at 50 hpf for 1 hour with a DMSO control.

Microscopy

Imaging fluorescent transgene expression in live embryos, antibody staining, and fluorescent staining was completed using an inverted laser scanning confocal microscope (LSM900; Zeiss) with a 10X (0.25 NA), 20X (0.8 NA), 40X water (1.1 NA) or 60X (1.4 NA) oil objectives. Laser wavelengths included blue (405), green (488), red (561), and far red (640). Embryos were maintained in PTU from 24 hpf onwards to prevent pigment development, anesthetized in 4% tricaine and mounted in 0.8% Low melt agarose dissolved in E3, on a clear imaging dish. In some cases, live samples were retrieved from the agarose following imaging for further imaging at later time points, genotyping, or other data collection. Images were processed using Zen Blue and Fiji (Schindelin et al., 2012) software.

Imaging of whole adult brains was completed using the Light-sheet microscope (Ultramicroscope II; LaVision Biotech) with a 2X (0.5 NA) objective at 1.0 zoom. Laser wavelengths included green (488) and red (561). Images were processed using Zen Blue, Fiji and Imaris software.

Pericyte Analysis

All pericyte metrics were analyzed using the Fiji counting or tracing tool on flattened Z-stacks from confocal images of the whole zebrafish head. Pericyte counting and analysis were restricted to the mid and hindbrain regions for all metrics. For pericyte process lengths, individual processes extending from one soma were measured and added together to determine the total process length per pericyte in μm. In instances where two processes appeared to merge or cover the same blood vessel, half of the total length was added to each pericyte. For Zebrabow images, only pericytes with processes distinguishable from neighbouring pericytes were measured. For soma size, individual cell bodies were traced, and the area was determined by the software in μm^2.

Vessel Metrics

Confocal images were analyzed using the Python-based software tool Vessel Metrics (McGarry et al., 2024). In general, the total vessel network length was measured starting from below the middle cerebral vein (MCeV) and dorsal longitudinal vein (DLV) until the emergence of the basal communicating artery (BCA). Vessels included in measurements as follows: middle mesencephalic central arteries (MMCtAs), posterior mesencephalic central arteries (PMCtAs), the primordial hindbrain channels (PHBCs) and the posterior region of the basilar artery (BA). The forebrain vessels (i.e. anterior cerebral veins (ACeVs) were not included). Blood vessel diameter was restricted to the horizontal hindbrain central arteries (CtAs), which were comparable between all images.

Statistics

All statistical analysis was completed using GraphPad Prism 10 software, with significance resulting from a p-value of <0.05. Statistical tests conducted are included in figure captions. The D'Agostino-Pearson test was used to assess the normality of data sets, and in cases where the data did not pass the normality test, non-parametric statistics were used. Experimental N's are located in Appendix A. Results are expressed on graphs as mean ± standard deviation (SD). Only significant p-values are indicated.

Acknowledgements

This work was funded by the Canadian Institutes of Health Research PJT-183631. MFG received a Canada Graduate Scholarship Master's from Canadian Institutes of Health Research, the Alberta Graduate Excellence Scholarship (AGES) for Master's Research from the Province of Alberta, and a Biochemistry and Molecular Biology Department scholarship from the University of Calgary. EH received the Alvin Libin Graduate Scholarship in Cardiovascular Research, the Alberta Children's Hospital Research Institute (ACHRI) Graduate Scholarship for Master's Research, the ACHRI Graduate Scholarship for Doctoral Research, and the Alberta Graduate Excellence Scholarship (AGES) for Doctoral Research from the Province of Alberta. We thank David Elliot for his insight and expertise in brain clearing and light-sheet imaging. We acknowledge the Alberta Children's Hospital Research Institute and Hotchkiss Brain Institute Imaging facilities for microscopes and technical support.

References

Ahuja, S., Adjekukor, C., Li, Q., Kocha, K. M., Rosin, N., Labit, E., Sinha, S., Narang, A., Long, Q., Biernaskie, J., et al. (2024). The development of brain pericytes requires expression of the transcription factor nkx3.1 in intermediate precursors. *PLoS Biol.* **22**, e3002590.

Arnold, C. R., Lamont, R. E., Walker, J. T., Spice, P. J., Chan, C., Ho, C. and Childs, S. J. (2015). Comparative analysis of genes regulated by Dzip1/ *iguana* and hedgehog in zebrafish. *Dev. Dyn.* **244**, 211–223.

Bahrami, N. and Childs, S. J. (2020). Development of vascular regulation in the zebrafish embryo. *Dev. Camb. Engl.* **147**, dev183061.

Becker, T., Wullimann, M. F., Becker, C. G., Bernhardt, R. R. and Schachner, M. (1997). Axonal regrowth after spinal cord transection in adult zebrafish. *J. Comp. Neurol.* **377**, 577–595.

Bell, R. D., Winkler, E. A., Sagare, A. P., Singh, I., LaRue, B., Deane, R. and Zlokovic, B. V. (2010). Pericytes control key neurovascular functions and neuronal phenotype in the adult brain and during brain aging. *Neuron* **68**, 409–427.

Berthiaume, A.-A., Hartmann, D. A., Majesky, M. W., Bhat, N. R. and Shih, A. Y. (2018a). Pericyte Structural Remodeling in Cerebrovascular Health and Homeostasis. *Front. Aging Neurosci.* **10**, 210.

Berthiaume, A.-A., Grant, R. I., McDowell, K. P., Underly, R. G., Hartmann, D. A., Levy, M., Bhat, N. R. and Shih, A. Y. (2018b). Dynamic Remodeling of Pericytes In Vivo Maintains Capillary Coverage in the Adult Mouse Brain. *Cell Rep.* **22**, 8–16.

Chauhan, G., Arnold, C. R., Chu, A. Y., Fornage, M., Reyahi, A., Bis, J. C., Havulinna, A. S., Sargurupremraj, M., Smith, A. V., Adams, H. H. H., et al. (2016). Identification of additional risk loci for stroke and small vessel disease: a meta-analysis of genome-wide association studies. *Lancet Neurol.* **15**, 695–707.

Chen, S., Francioli, L. C., Goodrich, J. K., Collins, R. L., Kanai, M., Wang, Q., Alföldi, J., Watts, N. A., Vittal, C., Gauthier, L. D., et al. (2024). A genomic mutational constraint map using variation in 76,156 human genomes. *Nature* **625**, 92–100.

Daneman, R., Zhou, L., Kebede, A. A. and Barres, B. A. (2010). Pericytes are required for blood-brain barrier integrity during embryogenesis. *Nature* **468**, 562–566.

Dave, J. M., Mirabella, T., Weatherbee, S. D. and Greif, D. M. (2018). Pericyte ALK5/TIMP3 Axis Contributes to Endothelial Morphogenesis in the Developing Brain. *Dev. Cell* **47**, 388–389.

Ding, R., Hase, Y., Ameen-Ali, K. E., Ndung'u, M., Stevenson, W., Barsby, J., Gourlay, R., Akinyemi, T., Akinyemi, R., Uemura, M. T., et al. (2020). Loss of capillary pericytes and the blood-brain barrier in white matter in poststroke and vascular dementias and Alzheimer's disease. *Brain Pathol. Zurich Switz.* **30**, 1087–1101.

Dukkipati, S. S., Garrett, T. L. and Elbasiouny, S. M. (2018). The vulnerability of spinal motoneurons and soma size plasticity in a mouse model of amyotrophic lateral sclerosis. *J. Physiol.* **596**, 1723–1745.

Duperron, M.-G., Knol, M. J., Le Grand, Q., Evans, T. E., Mishra, A., Tsuchida, A., Roshchupkin, G., Konuma, T., Trégouët, D.-A., Romero, J. R., et al. (2023). Genomics of perivascular space burden unravels early mechanisms of cerebral small vessel disease. *Nat. Med.* **29**, 950–962.

Eilken, H. M., Diéguez-Hurtado, R., Schmidt, I., Nakayama, M., Jeong, H.-W., Arf, H., Adams, S., Ferrara, N. and Adams, R. H. (2017). Pericytes regulate VEGF-induced endothelial sprouting through VEGFR1. *Nat. Commun.* **8**, 1574.

Fukui, K., Ushiki, K., Takatsu, H., Koike, T. and Urano, S. (2012). Tocotrienols prevent hydrogen peroxide-induced axon and dendrite degeneration in cerebellar granule cells. *Free Radic. Res.* **46**, 184–193.

Greenwood, S. M., Mizielinska, S. M., Frenguelli, B. G., Harvey, J. and Connolly, C. N. (2007). Mitochondrial dysfunction and dendritic beading during neuronal toxicity. *J. Biol. Chem.* **282**, 26235–26244.

Guo, D.-C., Papke, C. L., Tran-Fadulu, V., Regalado, E. S., Avidan, N., Johnson, R. J., Kim, D. H., Pannu, H., Willing, M. C., Sparks, E., et al. (2009). Mutations in smooth muscle alpha-actin (ACTA2) cause coronary artery disease, stroke, and Moyamoya disease, along with thoracic aortic disease. *Am. J. Hum. Genet.* **84**, 617–627.

Hill, R. A., Tong, L., Yuan, P., Murikinati, S., Gupta, S. and Grutzendler, J. (2015). Regional Blood Flow in the Normal and Ischemic Brain Is Controlled by Arteriolar Smooth Muscle Cell Contractility and Not by Capillary Pericytes. *Neuron* **87**, 95–110.

Kok, F. O., Shin, M., Ni, C.-W., Gupta, A., Grosse, A. S., van Impel, A., Kirchmaier, B. C., Peterson-Maduro, J., Kourkoulis, G., Male, I., et al. (2015). Reverse genetic screening reveals poor correlation between morpholino-induced and mutant phenotypes in zebrafish. *Dev. Cell* **32**, 97–108.

Kwon, C. H., Zhu, X., Zhang, J., Knoop, L. L., Tharp, R., Smeyne, R. J., Eberhart, C. G., Burger, P. C. and Baker, S. J. (2001). Pten regulates neuronal soma size: a mouse model of Lhermitte-Duclos disease. *Nat. Genet.* **29**, 404–411.

Kwon, C.-H., Zhu, X., Zhang, J. and Baker, S. J. (2003). mTor is required for hypertrophy of Pten-deficient neuronal soma in vivo. *Proc. Natl. Acad. Sci. U. S. A.* **100**, 12923–12928.

Lepilina, A., Coon, A. N., Kikuchi, K., Holdway, J. E., Roberts, R. W., Burns, C. G. and Poss, K. D. (2006). A dynamic epicardial injury response supports progenitor cell activity during zebrafish heart regeneration. *Cell* **127**, 607–619.

McGarry, S. D., Adjekukor, C., Ahuja, S., Greysson-Wong, J., Vien, I., Rinker, K. D. and Childs, S. J. (2024). Vessel Metrics: A software tool for automated analysis of vascular structure in confocal imaging. *Microvasc. Res.* **151**, 104610.

Østergaard, L., Engedal, T. S., Moreton, F., Hansen, M. B., Wardlaw, J. M., Dalkara, T., Markus, H. S. and Muir, K. W. (2016). Cerebral small vessel disease: Capillary pathways to stroke and cognitive decline. *J. Cereb. Blood Flow Metab. Off. J. Int. Soc. Cereb. Blood Flow Metab.* **36**, 302–325.

Otteson, D. C. and Hitchcock, P. F. (2003). Stem cells in the teleost retina: persistent neurogenesis and injury-induced regeneration. *Vision Res.* **43**, 927–936.

Pan, Y. A., Freundlich, T., Weissman, T. A., Schoppik, D., Wang, X. C., Zimmerman, S., Ciruna, B., Sanes, J. R., Lichtman, J. W. and Schier, A. F. (2013). Zebrabow: multispectral cell labeling for cell tracing and lineage analysis in zebrafish. *Dev. Camb. Engl.* **140**, 2835–2846.

Reyahi, A., Nik, A. M., Ghiami, M., Gritli-Linde, A., Pontén, F., Johansson, B. R. and Carlsson, P. (2015). Foxf2 Is Required for Brain Pericyte Differentiation and Development and Maintenance of the Blood-Brain Barrier. *Dev. Cell* **34**, 19–32.

Rouf, M. A., Wen, L., Mahendra, Y., Wang, J., Zhang, K., Liang, S., Wang, Y., Li, Z., Wang, Y. and Wang, G. (2023). The recent advances and future perspectives of genetic compensation studies in the zebrafish model. *Genes Dis.* **10**, 468–479.

Rousseau, V., Engelmann, R. and Sabel, B. A. (1999). Restoration of vision III: soma swelling dynamics predicts neuronal death or survival after optic nerve crush in vivo. *Neuroreport* **10**, 3387–3391.

Ryu, J.-R., Ahuja, S., Arnold, C. R., Potts, K. G., Mishra, A., Yang, Q., Sargurupremraj, M., Mahoney, D. J., Seshadri, S., Debette, S., et al. (2022). Stroke-associated intergenic variants modulate a human FOXF2 transcriptional enhancer. *Proc. Natl. Acad. Sci. U. S. A.* **119**, e2121333119.

Schindelin, J., Arganda-Carreras, I., Frise, E., Kaynig, V., Longair, M., Pietzsch, T., Preibisch, S., Rueden, C., Saalfeld, S., Schmid, B., et al. (2012). Fiji: an open-source platform for biological-image analysis. *Nat. Methods* **9**, 676–682.

Seiradake, E., Jones, E. Y. and Klein, R. (2016). Structural Perspectives on Axon Guidance. *Annu. Rev. Cell Dev. Biol.* **32**, 577–608.

Stratman, A. N., Malotte, K. M., Mahan, R. D., Davis, M. J. and Davis, G. E. (2009). Pericyte recruitment during vasculogenic tube assembly stimulates endothelial basement membrane matrix formation. *Blood* **114**, 5091–5101.

Sur, A., Wang, Y., Capar, P., Margolin, G. and Farrell, J. A. (2023). Single-cell analysis of shared signatures and transcriptional diversity during zebrafish development. *BioRxiv Prepr. Serv. Biol.* 2023.03.20.533545.

Vanlandewijck, M., He, L., Mäe, M. A., Andrae, J., Ando, K., Del Gaudio, F., Nahar, K., Lebouvier, T., Laviña, B., Gouveia, L., et al. (2018). A molecular atlas of cell types and zonation in the brain vasculature. *Nature* **554**, 475–480.

Wang, Y., Pan, L., Moens, C. B. and Appel, B. (2014). Notch3 establishes brain vascular integrity by regulating pericyte number. *Dev. Camb. Engl.* **141**, 307–317.

Westerfield, M. (2007). *THE ZEBRAFISH BOOK, 5th Edition; A guide for the laboratory use of zebrafish (Danio rerio)*. Eugene: University of Oregon Press.

Whitesell, T. R., Chrystal, P. W., Ryu, J.-R., Munsie, N., Grosse, A., French, C. R., Workentine, M. L., Li, R., Zhu, L. J., Waskiewicz, A., et al. (2019). foxc1 is required for embryonic head vascular smooth muscle differentiation in zebrafish. *Dev. Biol.* **453**, 34–47.

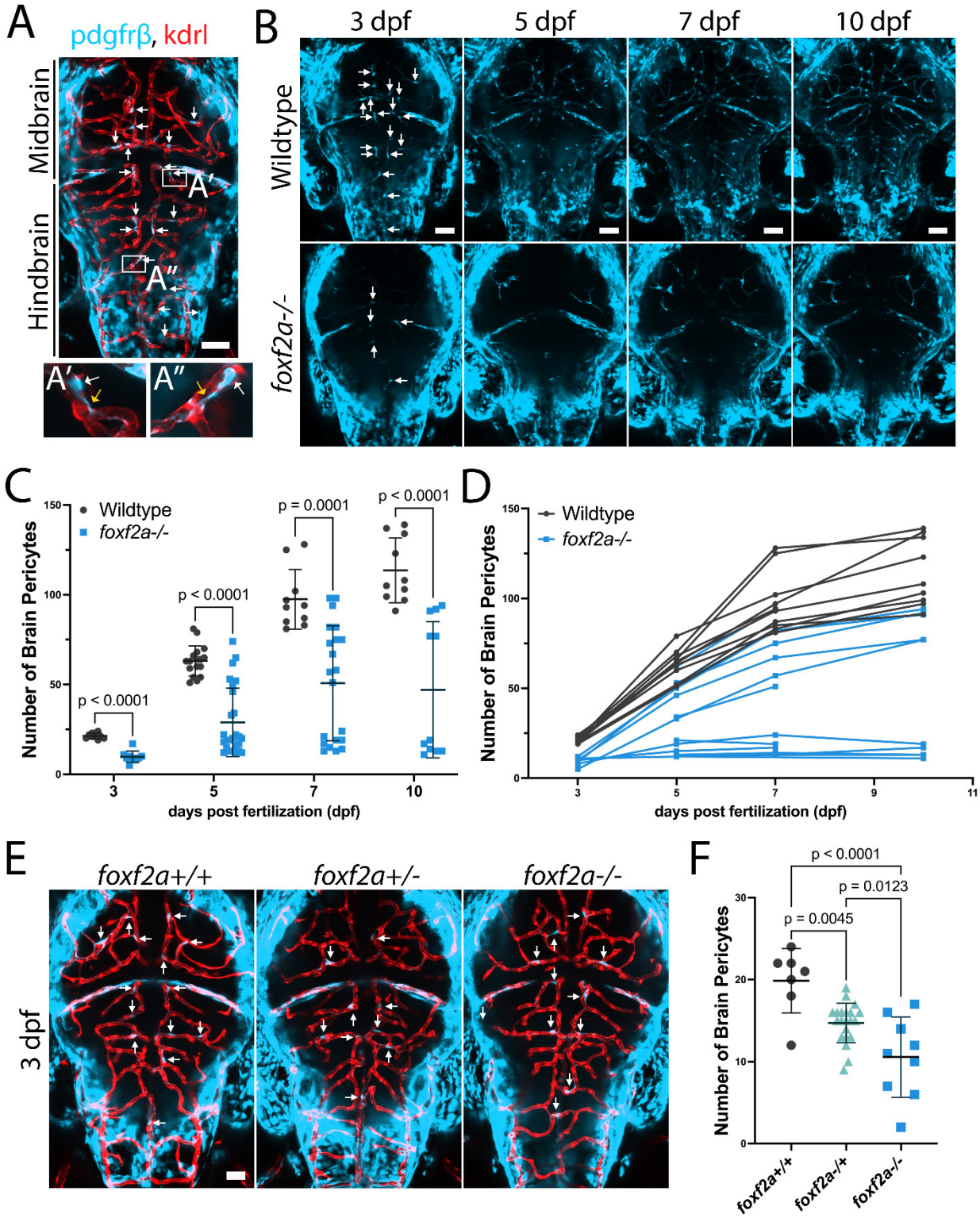

Figure 1. Brain pericyte number is consistently lower and does not recover in *foxf2a* mutant larvae. (A) Zebrafish brains were imaged using endothelial (red; *Tg(kdrl:mCherry)*) and pericyte (light blue; *Tg(pdgfrβ:Gal4, UAS:GFP)*) transgenic lines (arrows: brain pericytes). (A'-A'') Brain pericyte soma (white arrows) and processes (yellow arrows) are closely associated with the endothelium. (B) Serially imaged wildtype and *foxf2a* mutant brains at 3, 5, 7 and 10 dpf. (C) Total brain pericyte numbers at 3, 5, 7 and 10 dpf. (D) Individual brain pericyte trajectories of serially imaged embryos over the same period. (E) Dorsal images of embryos for the indicated genotypes from a *foxf2a*

heterozygous incross at 75 hpf. (F) Total brain pericytes at 75 hpf. Statistical analysis was conducted using multiple Mann-Whitney tests (C) and one-way ANOVA with Tukey's test (F). Scale bars, 50 μm (A-B, E).

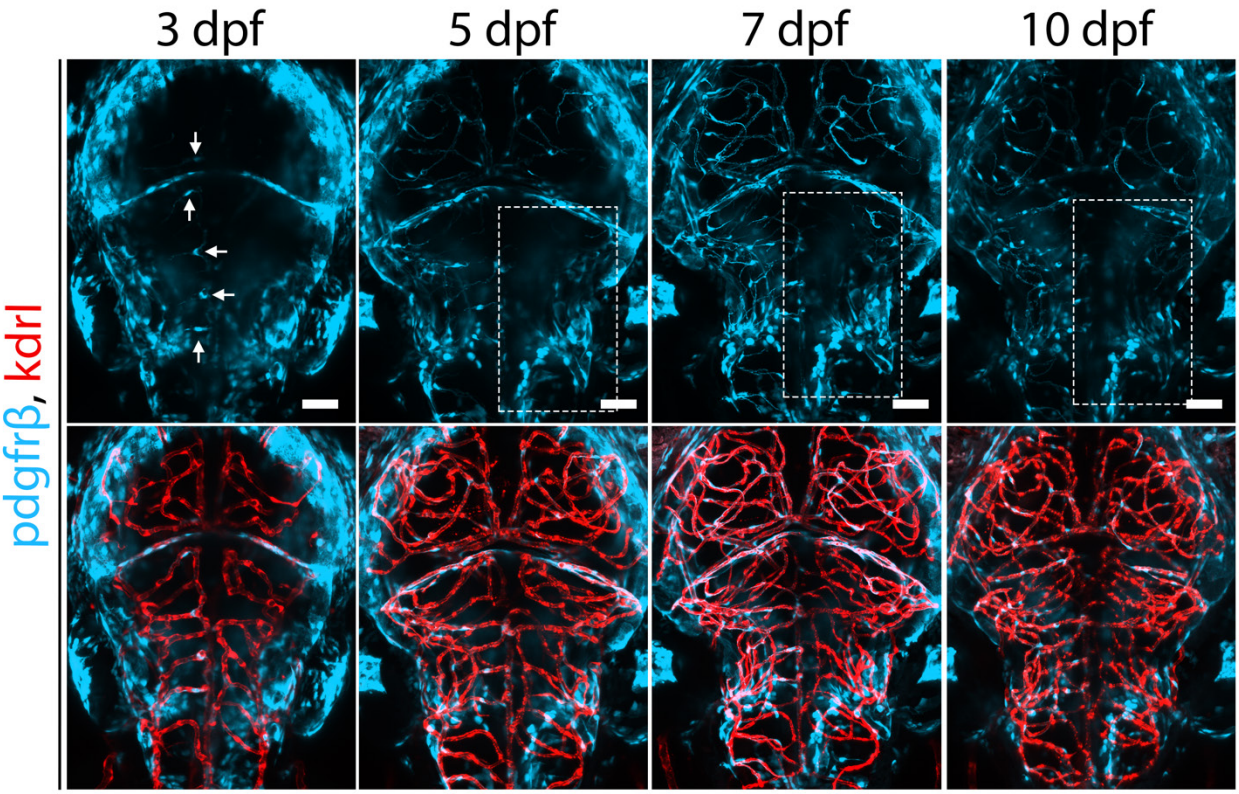

Supplemental Figure 1. *foxf2a* mutants exhibit regional loss. Serial imaging of a *foxf2a-/-* mutant brain at 3, 5, 7 and 10 dpf (arrows: brain pericytes; boxes: regional loss). Scale bars, 50 µm.

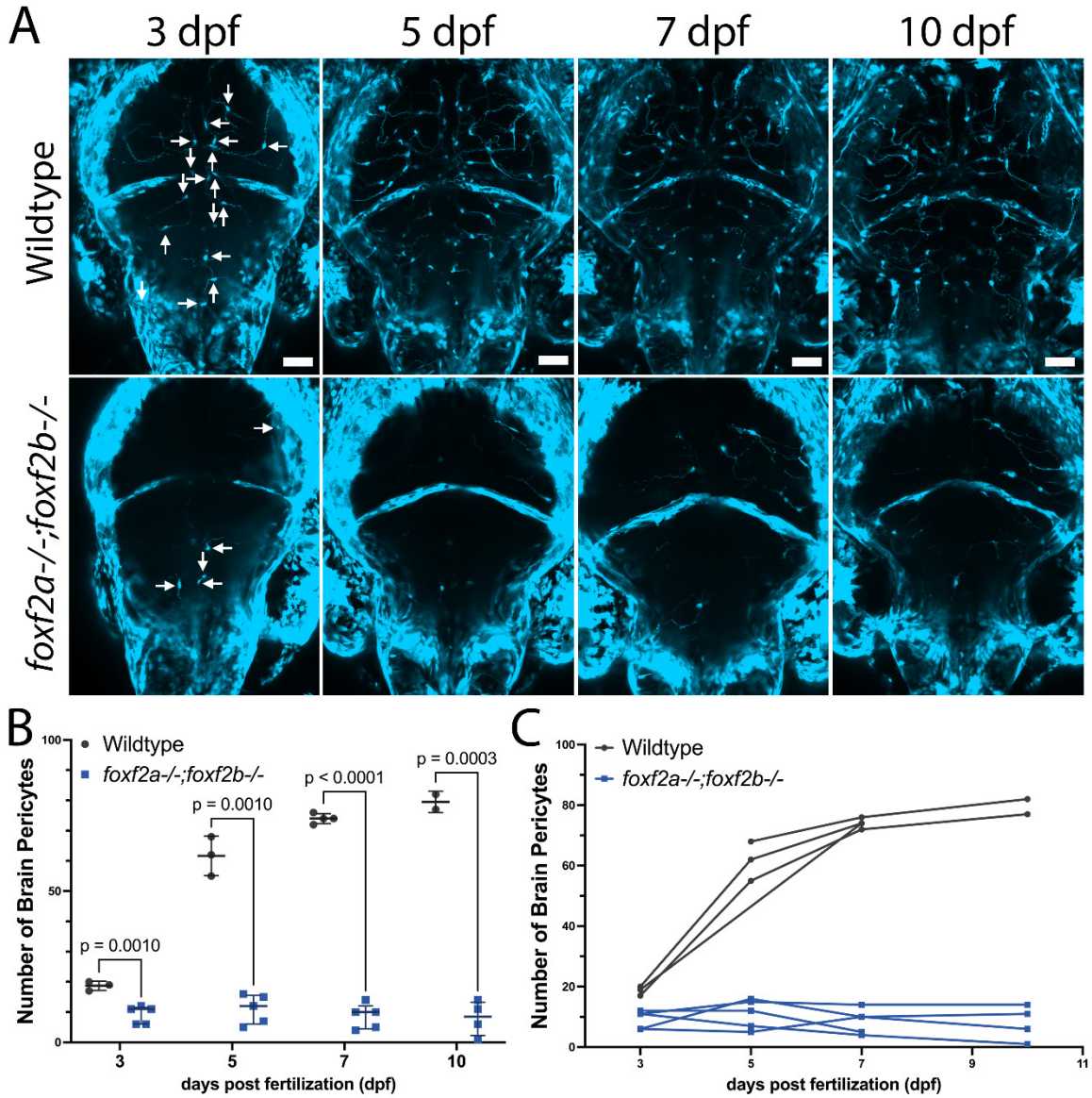

Supplemental Figure 2. foxf2 knockouts have severe pericyte deficiency during development. (A) Serial imaging of wildtype and *foxf2a-/-;foxf2b-/-* double mutant brains at 3, 5, 7 and 10 dpf (arrows: brain pericytes). (B) Scatter plot of total brain pericyte numbers at 3, 5, 7 and 10 dpf. (C) Individual mutant trajectories over the same period. Statistical analysis was conducted using multiple unpaired t-tests with Welch corrections. Scale bars, 50 μm (A).

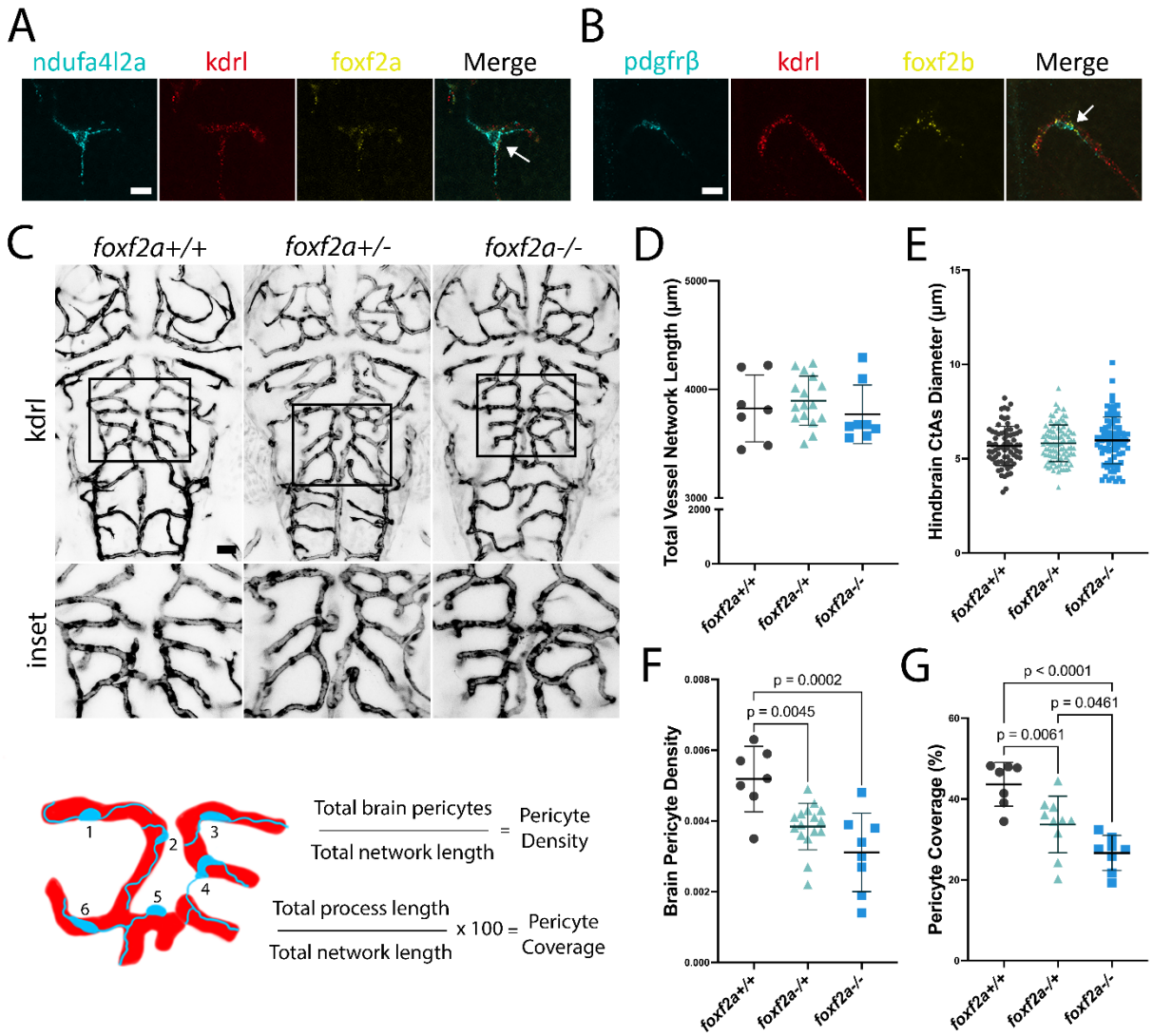

Figure 2. *Foxf2* affects embryonic pericyte numbers, but not endothelial cell pattern. (A-B) Expression of *foxf2* in a wildtype brain at 72 hpf using Hybridization Chain Reaction (HCR) is co-expressed with pericyte markers. (A) *foxf2a* is co-expressed with pericyte marker *ndufa4l2a* (arrows show overlapping expression). (B) *foxf2b* is co-expressed with pericyte marker *pdgfrβ* but also lowly expressed in the endothelium (*kdrl*) (arrow shows overlapping expression with endothelium). (C) Endothelium used to generate the total blood vessel network length. (D) Total vessel network length from Vessel Metrics software. (E) Scatter plot of hindbrain CtA diameters. (F) Scatter plot of pericyte density and pericyte coverage (G). Statistical analysis was conducted using one-way ANOVA with Tukey's test. Scale bars, 10 µm (A), 50 µm (C).

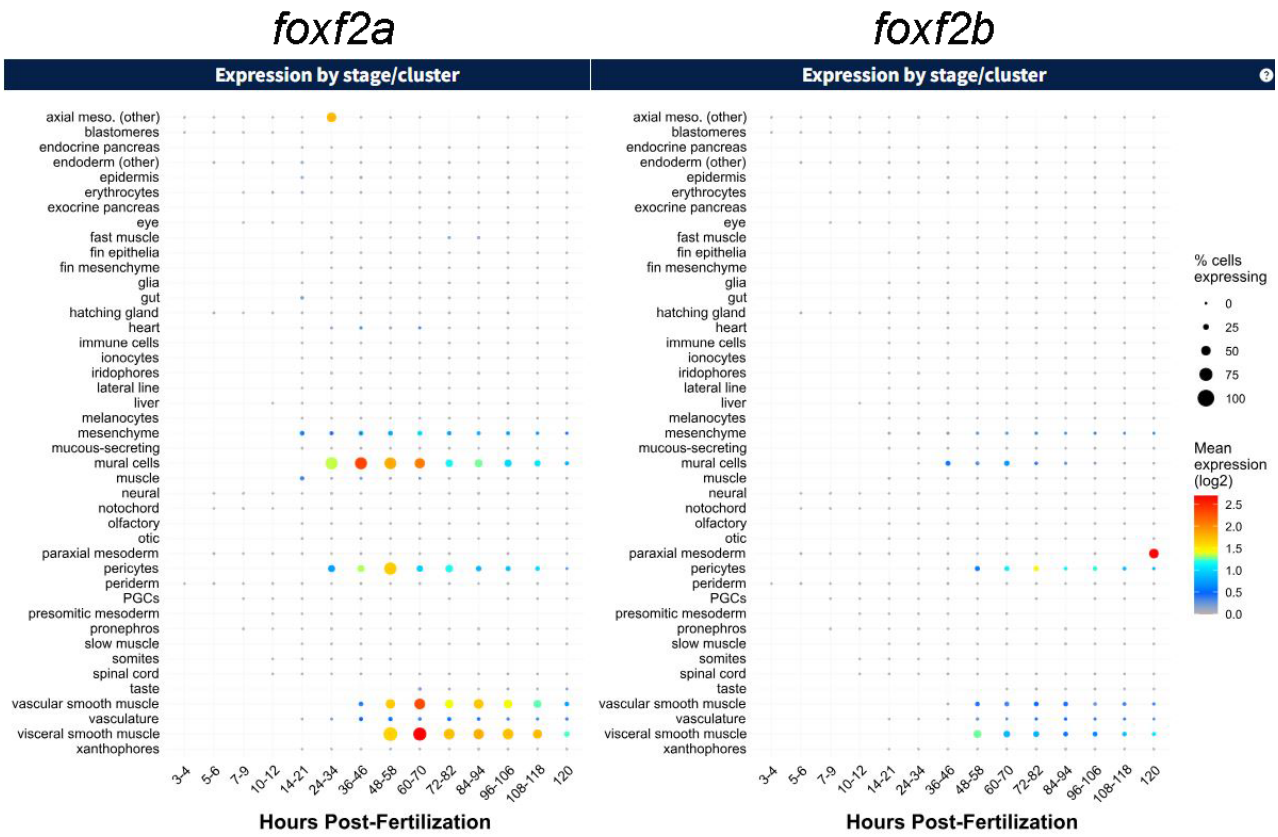

Supplemental Figure 3: Expression of *foxf2a* and *foxf2b* in single-cell sequencing data from Daniocell. *foxf2a* is expressed strongly in mural cells, pericytes and smooth muscle (vascular and visceral), with lower expression of *foxf2b* in the same cell types. Available at: https://daniocell.nichd.nih.gov/.

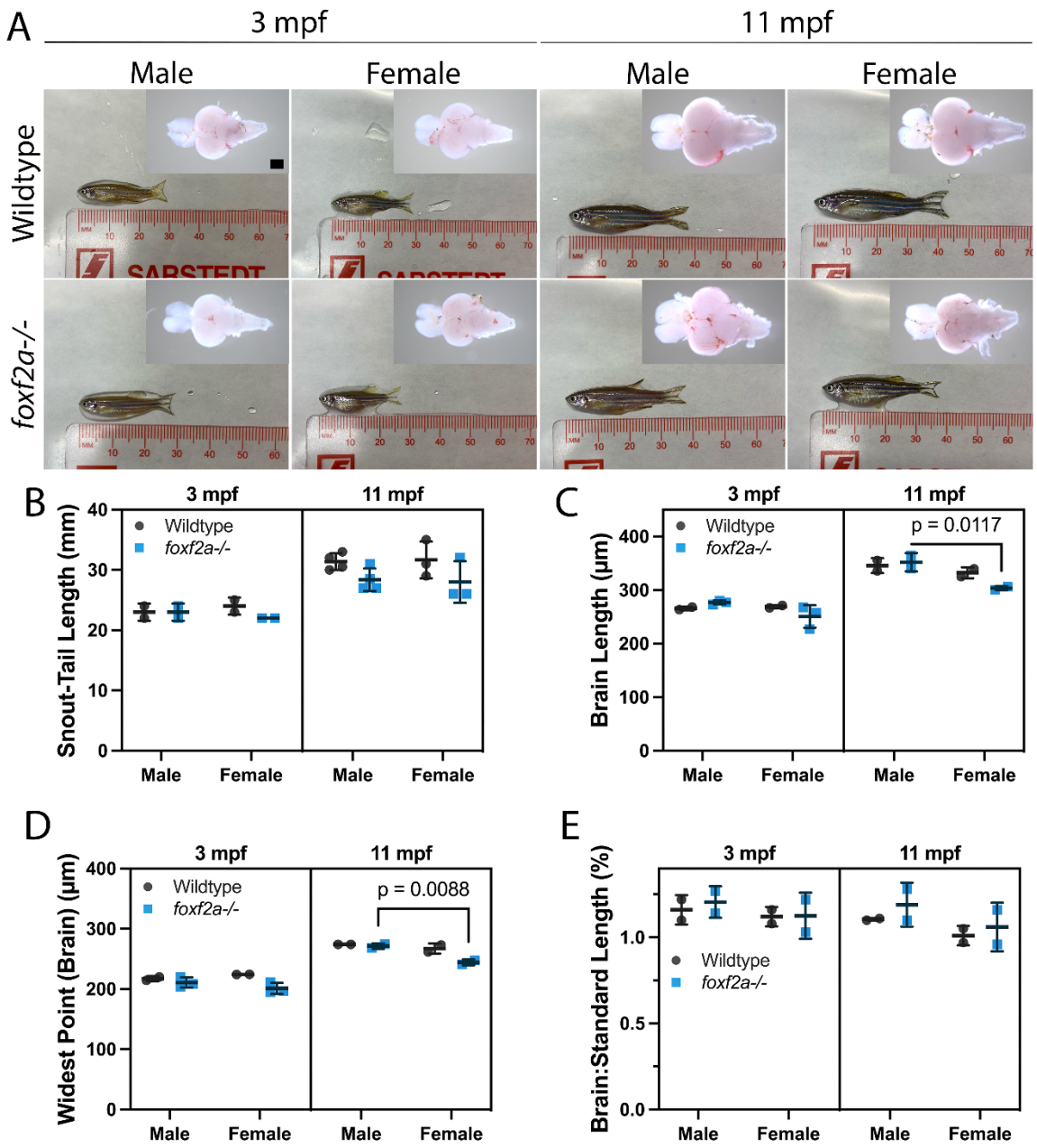

Supplemental Figure 4. *foxf2a mutant* adult brains have normal size as compared to wildtypes. (A) 3-month-old and 11-month-old *foxf2a*$^{-/-}$ mutant and wildtype brains were dissected and imaged dorsally under Brightfield. (B) Standard length measured from snout to base of the tail. (C) Brain length was measured from the tip of the forebrain to the end of the cerebellum. (D) Widest portion of midbrain measured. (E) Ratio of brain length relative to standard length. Statistical analysis was conducted using two-way ANOVAs with Šídák's multiple comparison test. Scale bars, 50 µm (A).

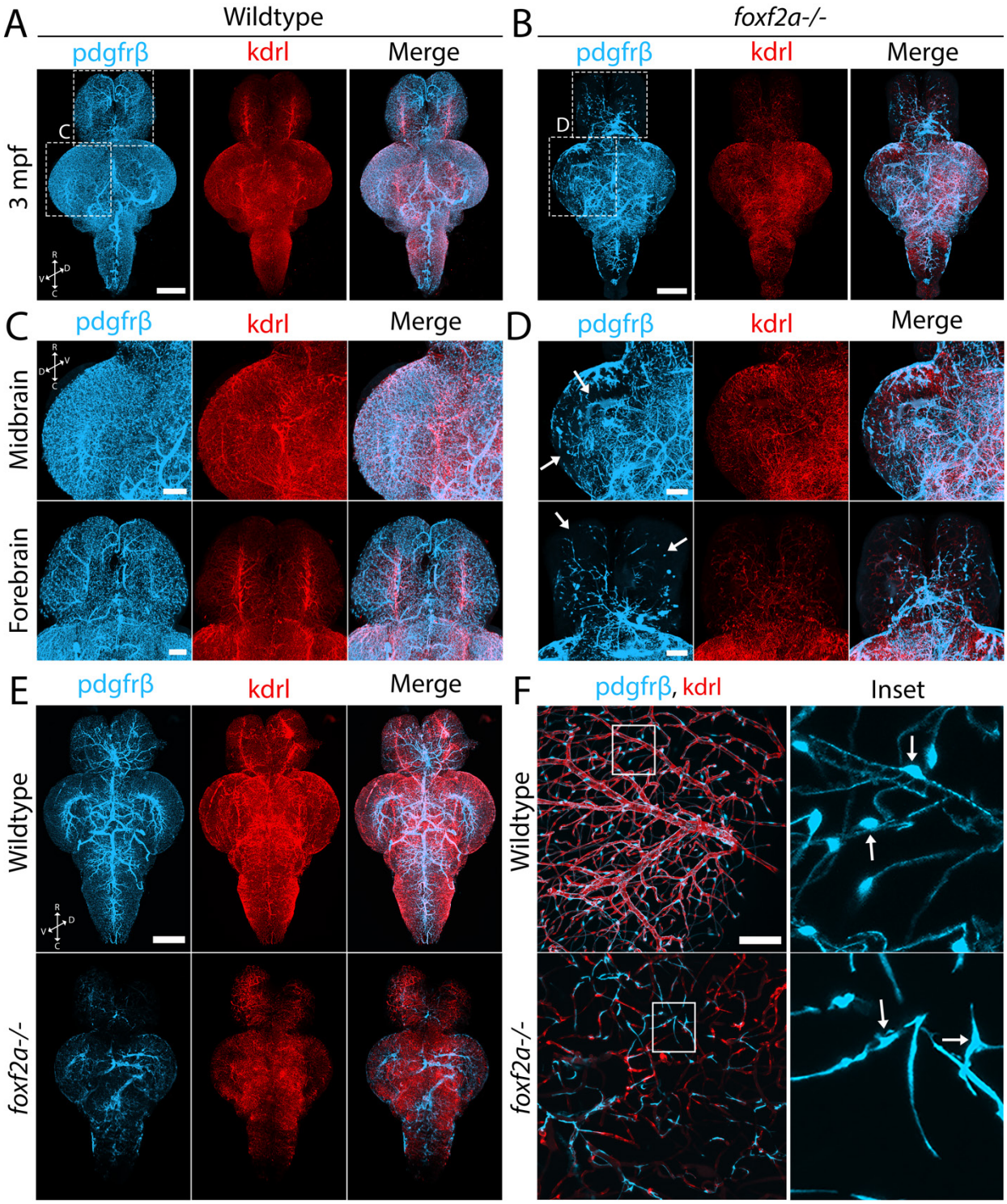

Figure 3. *foxf2a* mutants show strong brain vascular defects as adults. (A-B) 3D projections of iDISCO-cleared immunostained whole wildtype and *foxf2a*$^{-/-}$ brains at 3 mpf, viewed ventrally. (C-D) Wildtype and *foxf2a* mutant 2 brain regions, viewed dorsally (arrows = defects in coverage). (E) 3D projections of CUBIC-cleared whole wildtype and *foxf2a*$^{-/-}$ brains at 11 mpf with *Tg(pdgfrβ:Gal4, UAS:GFP, kdrl:mCherry)* viewed ventrally. (F) CUBIC-cleared wildtype and *foxf2a* mutant midbrain at 11 mpf (arrows: individual pericyte soma). C = caudal, D = dorsal, R = rostral, V = ventral. Scale bars, 500 µm (A-B), 200 µm (C-D), 700 µm (E), 50 µm (F).

Movie 1. Rotating view of a cleared wildtype brain (sample 1) at 3 mpf with *pdgfr*β (blue) and *kdrl* (red).

Movie 2. Rotating view of a cleared foxf2a mutant brain (sample 2) at 3 mpf with *pdgfr*β (blue) and *kdrl* (red).

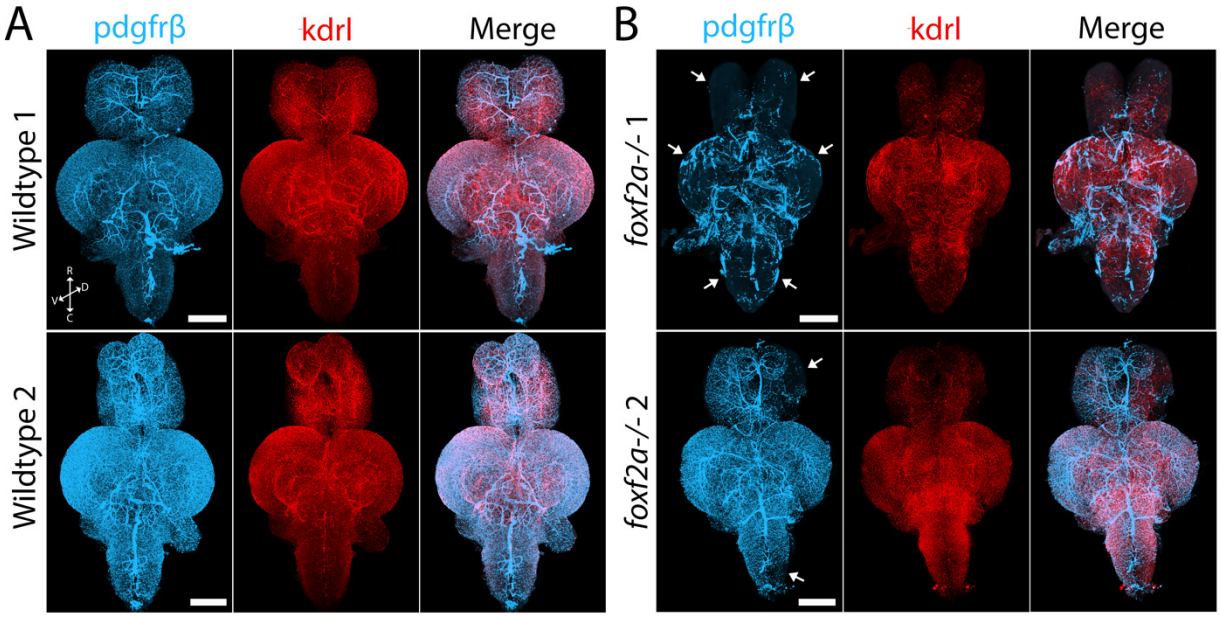

Supplemental Figure 5. *foxf2a* mutants show strong brain vascular defects in early adulthood. (A-B) 3D projections of iDISCO-cleared immunostained whole wildtype and *foxf2a*$^{-/-}$ brains at 3 mpf, viewed ventrally (arrows = defects in coverage). R = rostral, C = caudal, D = dorsal, V = ventral. Scale bars, 500 µm (A-B).

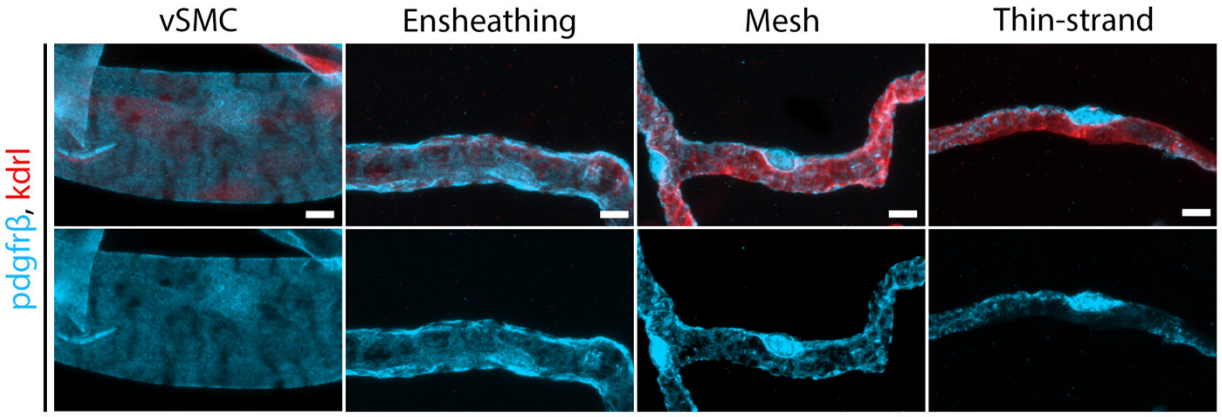

Supplemental Figure 6. Pericyte heterogeneity in the adult zebrafish brain. Immunolabeling for mural cell transgenes (*kdrl:mCherry and pdgfr*β*:Gal4, UAS:GFP*) on zebrafish brain vibratome sections. Vascular smooth muscle cells (vSMC), and pericyte (ensheathing, mesh and thin strand) subtypes are present in the adult zebrafish brain. Scale bars, 5 µm.

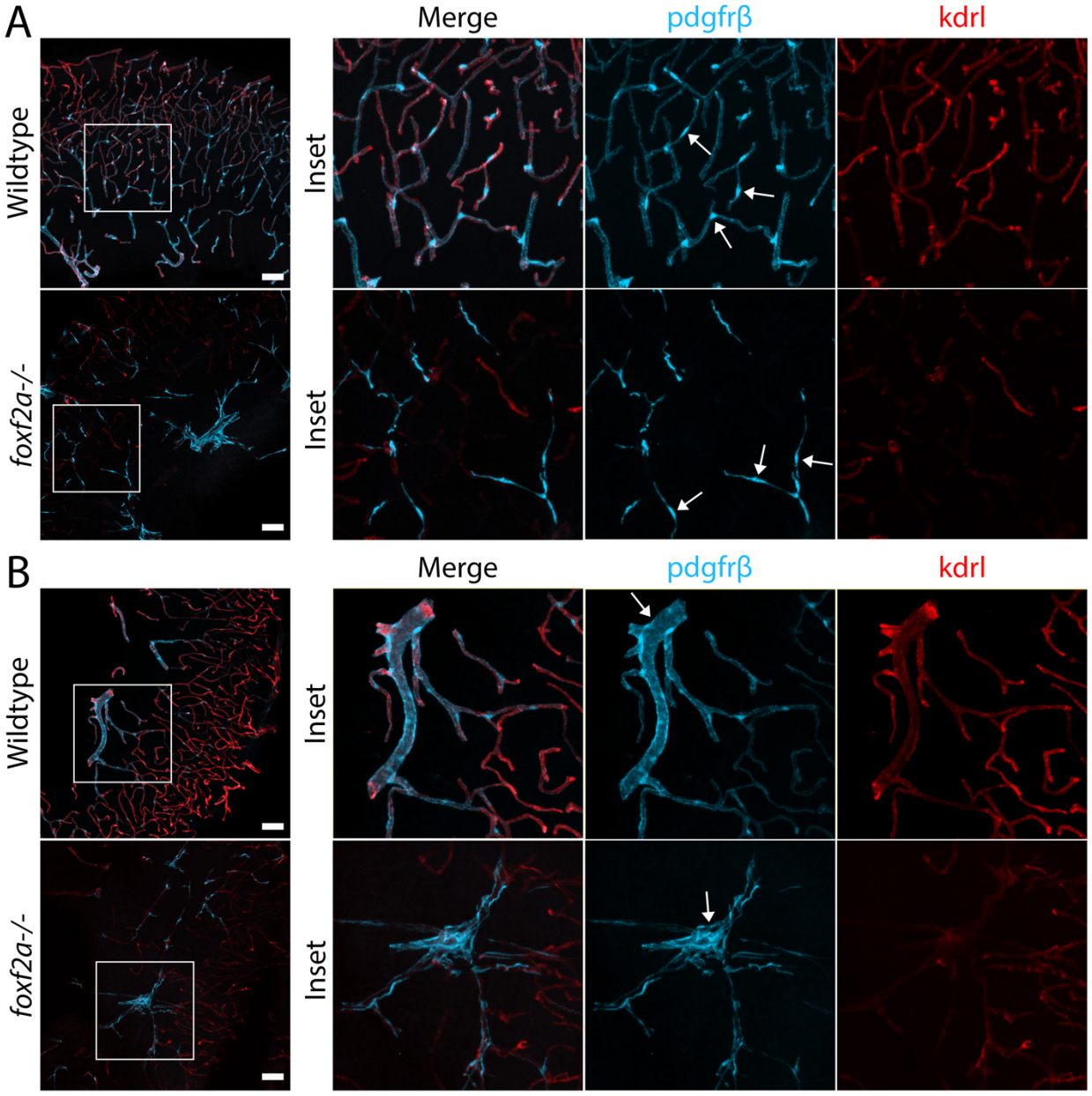

Figure 4. *foxf2a* mutants show unusual *pdgfrβ*-expressing cells and blood vessels in the adult brain. Immunolabeled sections in equivalent regions of wildtype and *foxf2a*$^{-/-}$ mutant brains at 11 mpf. (A) Region of the brain with an inset of *pdgfrβ*-expressing mural cells, likely vSMCs (arrows: large calibre vessel). (B) Region of the brain with an inset of pericytes (arrows: individual cell bodies. Scale bars, 50 μm (A-B).

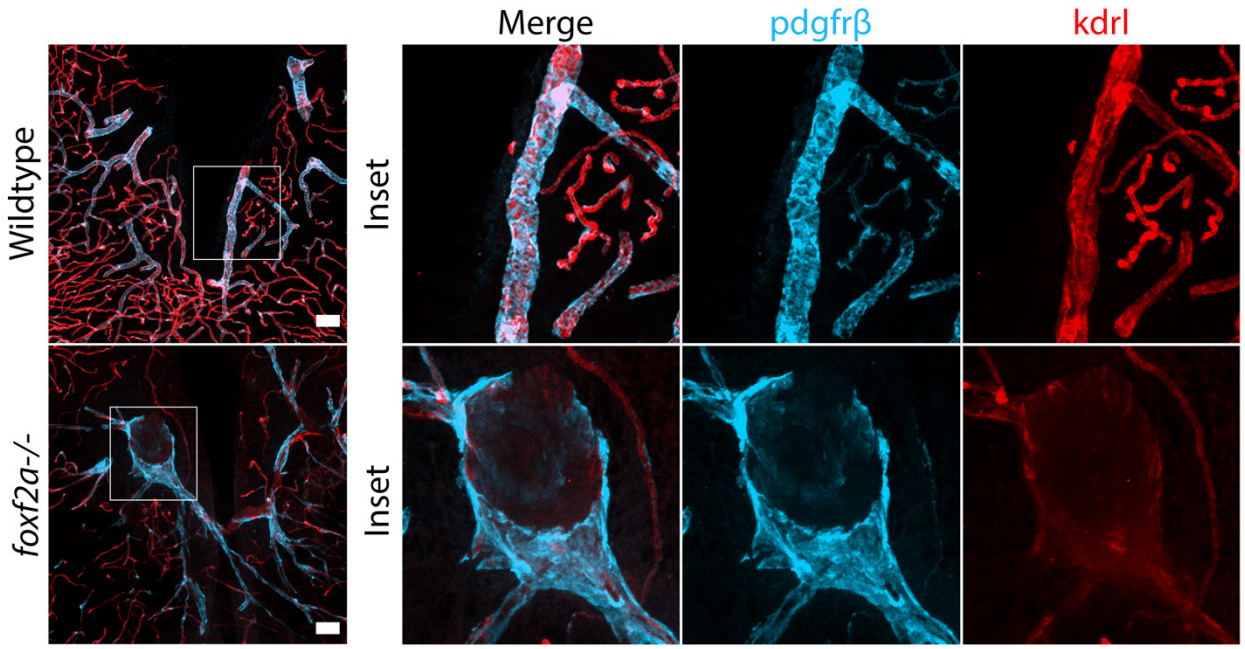

Supplemental Figure 7. Abnormal blood vessels become apparent in adult *foxf2a* mutant brains. Immunolabeled sections in equivalent regions of wildtype and *foxf2a*$^{-/-}$ mutant brains at 11 mpf. Large aneurysm-like structure with downregulated *kdrl* compared to the matched wildtype region. Scale bars, 50 μm (A-B).

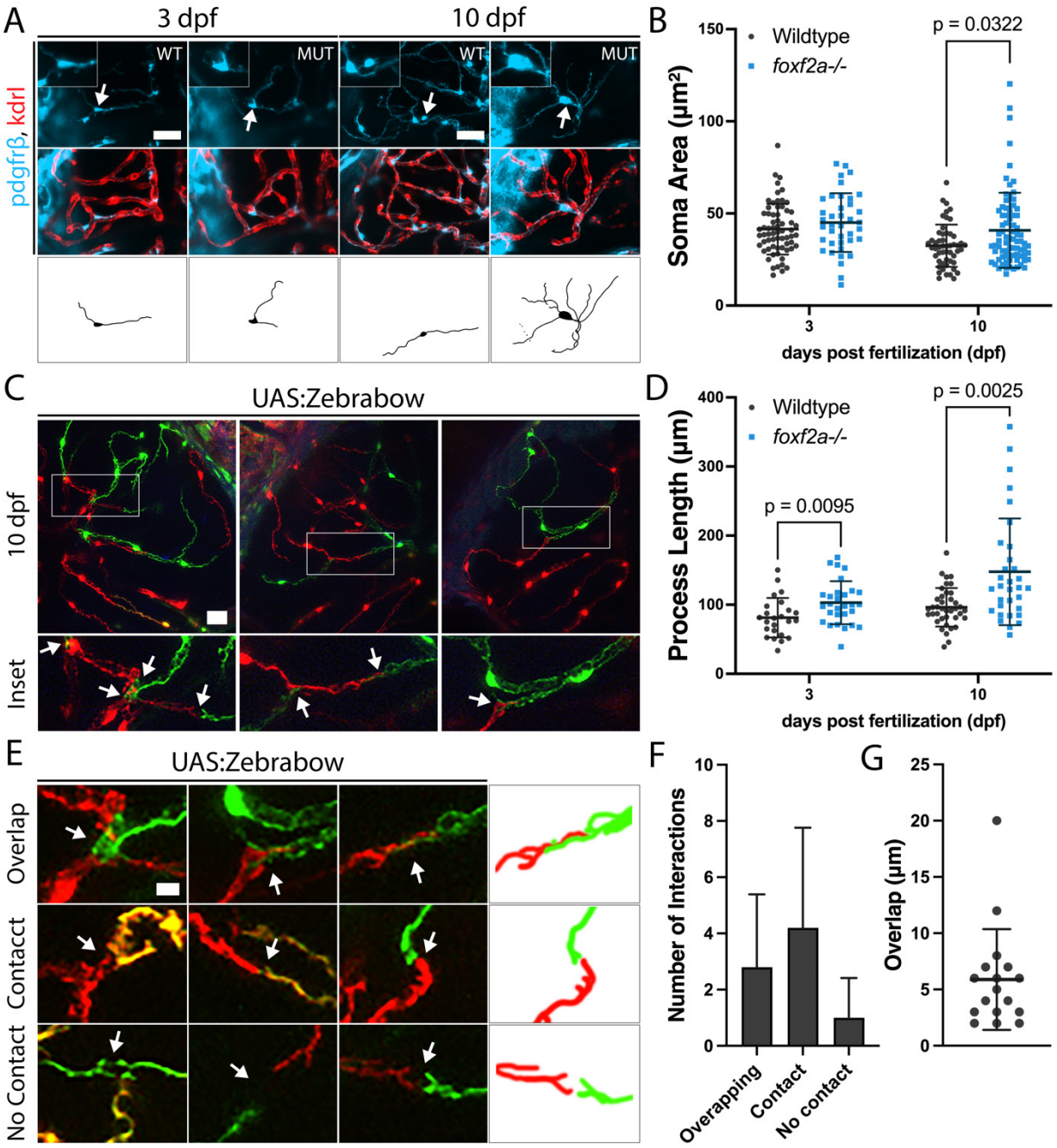

Figure 5. *foxf2a* mutant brain pericytes show increased soma size and process length. (A) Wildtype and *foxf2a*$^{-/-}$ mutant brain pericytes at 3 and 10 dpf with tracings of individual pericytes (indicated by arrows). (B) Brain pericyte soma area at 3 and 10 dpf. (C) Multispectral Zebrabow labelling reveals pericyte-process interactions in the larval brain. (arrows: pericyte interaction points). (D) Total process length per pericyte at 3 and 10 dpf. (E) Varying pericyte-pericyte interactions at 10 dpf (arrows: interaction points). (F) Number of each type of interaction at 10 dpf. (G) Length of overlap when process interaction occurs.Statistical analysis was conducted using multiple Mann-Whitney tests in B, a one-way ANOVA with Tukey's test at 3 dpf and a Kruskal-Wallis test with Dunn's multiple comparisons test at 10 dpf in D. Scale bars, 25 μm (A), 20 μm (C), 5 μm (E).

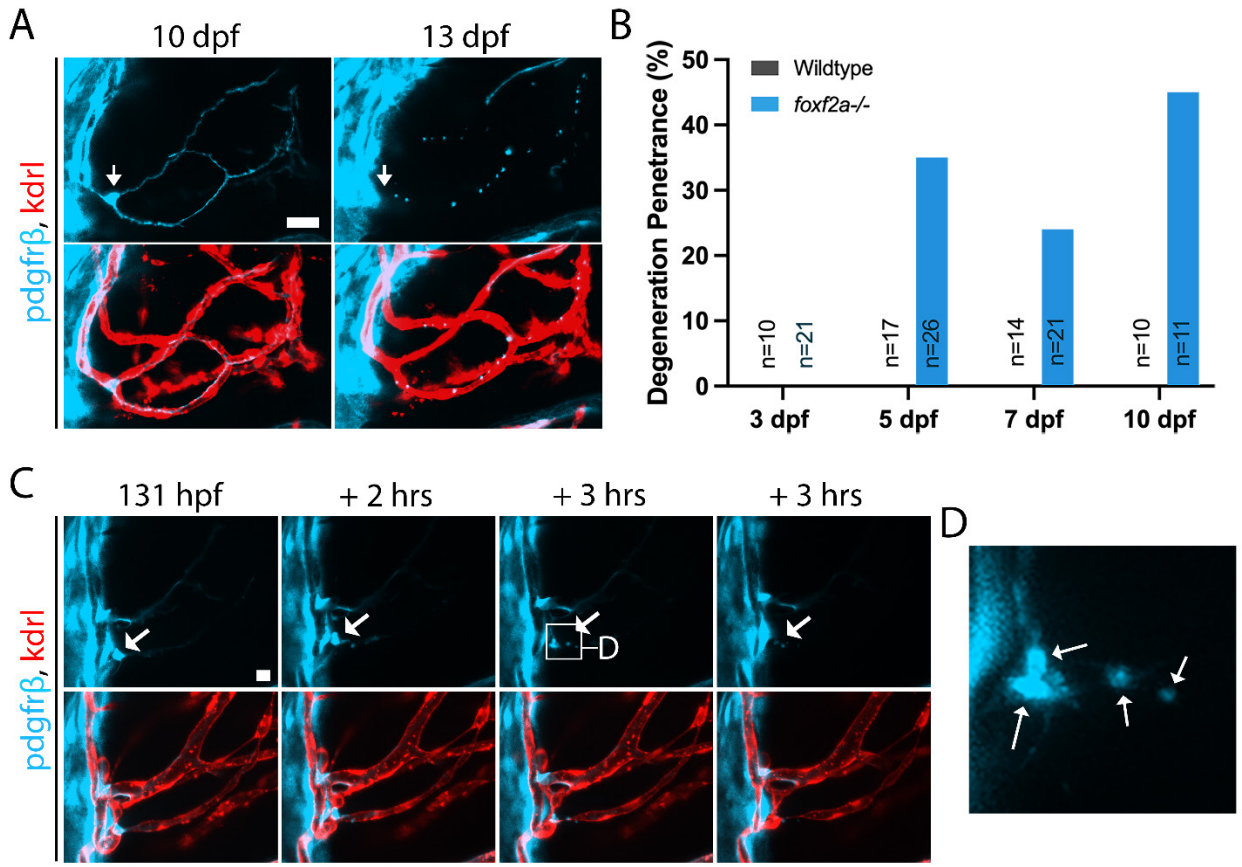

Figure 6. *foxf2a* mutant pericytes degenerate. (A) *foxf2a*$^{-/-}$ mutant pericyte at 10 and 13 dpf with the degenerating process and cell body (arrows: individual pericyte). (B) Bar graph with process blebbing phenotype penetrance in wildtype and mutant brains (n = total samples examined). (C) Timelapse of a *foxf2a*$^{-/-}$ mutant midbrain from 4-5 dpf (arrows: individual pericyte). (D) Inset of mutant pericyte undergoing degeneration (arrows: blebbing). Scale bars, 20 μm (A, C).

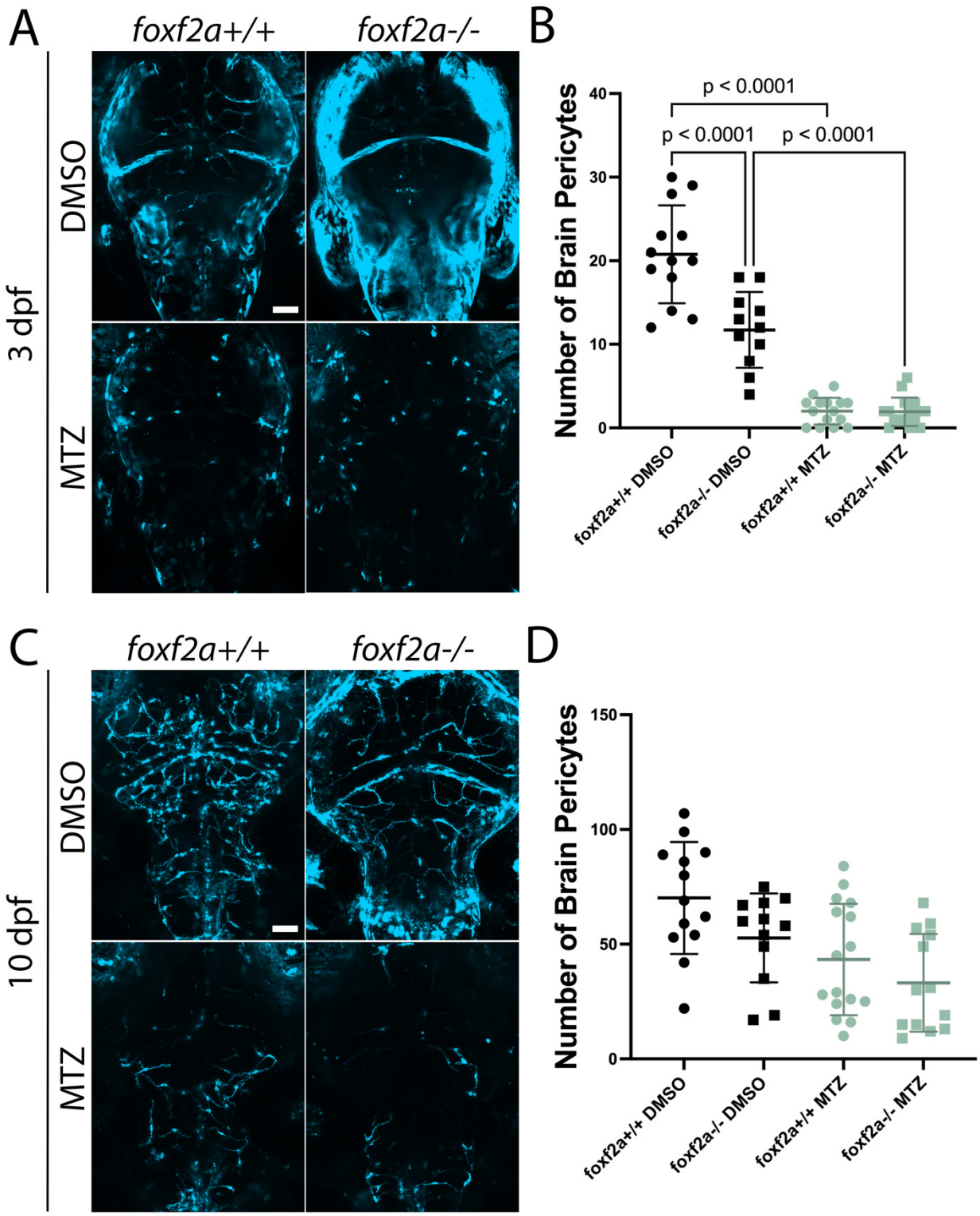

Figure 7. *foxf2a* mutants do not have impaired regeneration of brain pericytes after genetic ablation. Zebrafish brains were imaged using endothelial (red; *Tg(kdrl:GFP)*) and pericyte (light blue; *Tg(pdgfrβ:Gal4, UAS:NTR-mCherry)*) transgenic lines. (A) Wildtype and mutant brains at 3 dpf in control (DMSO) and treated (MTZ) groups. (B) Total brain pericytes at 3 dpf. (C) Wildtype and mutant brains at 10 dpf. (D) Total brain pericytes at 10 dpf. Statistical analysis was conducted using a one-way ANOVA (B) or Kruskal-Wallis test with Dunn's multiple comparisons test (D). Scale bars, 50 μm (A, C).

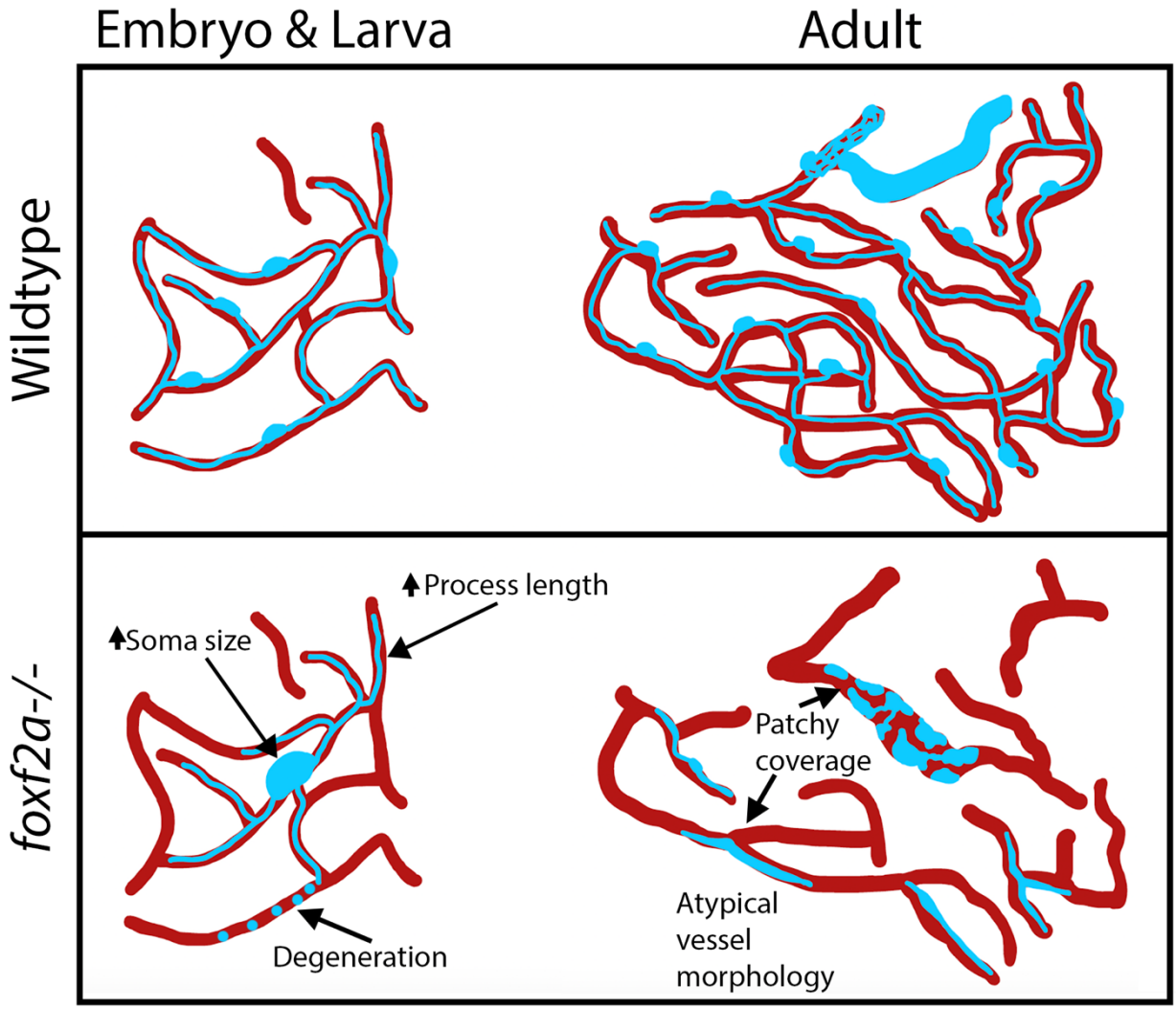

Figure 8. Model of *foxf2a* mutant brain pericyte defects over the lifespan. Wildtype pericytes develop normally in the embryo and establish extensive, continuous coverage over vessels by adulthood. *foxf2a* mutant pericytes exhibit abnormal morphology during development that changes over the lifespan, leaving mutant vasculature severely affected.